Cell. Mol. Life Sci. (2011) 68:3109–3120
DOI 10.1007/s00018-010-0615-0

Cellular and Molecular Life Sciences

RESEARCH ARTICLE

# Light on the structure of thromboxane $A_2$ receptor heterodimers

**Francesca Fanelli · Mario Mauri · Valérie Capra · Francesco Raimondi · Francesca Guzzi · Manuela Ambrosio · G. Enrico Rovati · Marco Parenti**

Received: 26 July 2010 / Revised: 16 November 2010 / Accepted: 14 December 2010 / Published online: 7 January 2011


**Abstract** The structure-based design of a mutant form of the thromboxane $A_2$ prostanoid receptor (TP) was instrumental in characterizing the structural determinants of the hetero-dimerization process of this G protein coupled receptor (GPCR). The results suggest that the heterodimeric complexes between the TP$\alpha$ and $\beta$ isoforms are characterized by contacts between hydrophobic residues in helix 1 from both monomers. Functional characterization confirms that TP$\alpha$–TP$\beta$ hetero-dimerization serves to regulate TP$\alpha$ function through agonist-induced internalization, with important implications in cardiovascular homeostasis. The integrated approach employed in this study can be adopted to gain structural and functional insights into the dimerization/oligomerization process of all GPCRs for which the structural model of the monomer can be achieved at reasonable atomic resolution.

**Electronic supplementary material** The online version of this article (doi:10.1007/s00018-010-0615-0) contains supplementary material, which is available to authorized users.

F. Fanelli (✉)
Department of Chemistry, Dulbecco Telethon Institute, University of Modena and Reggio Emilia, via Campi 183, 41100 Modena, Italy
e-mail: fanelli@unimo.it

F. Fanelli · F. Raimondi
Department of Chemistry, University of Modena and Reggio Emilia, Modena, Italy

M. Mauri · F. Guzzi · M. Parenti
Department of Experimental Medicine, University of Milano-Bicocca, Monza, Italy

V. Capra · M. Ambrosio · G. Enrico Rovati
Laboratory of Molecular Pharmacology, Department of Pharmacological Sciences, University of Milano, Milan, Italy

**Keywords** GPCR dimerization · Prostanoid receptors · Quaternary structure prediction · Protein–protein docking · Molecular recognition

## Introduction

G protein coupled receptors (GPCRs) comprise the largest family of signal transducing proteins that account for up to 40% of the total targets for existing drugs (reviewed in [1]). Emerging evidence suggests that many GPCRs exist as homo- and/or hetero-assemblies of two or more monomers [2, 3]. The thromboxane $A_2$ receptor (TP) is not an exception, as in vitro evidence has shown that the $\alpha$ and $\beta$ isoforms of this GPCR form homodimers and heterodimers independently from their functional state (this study and the papers from [4, 5], as well as heterodimers with other prostanoid GPCRs [6, 7]. Owing to the key roles played by TP for maintaining cardiovascular homeostasis as well as for its involvement in major cardiovascular events, such as myocardial infarction, thrombosis, and altered vessel wall reactivity [8], it is essential to shed some light on the role of dimerization/oligomerization in the functioning and regulation of this receptor.

In spite of the evidence that rhodopsin and the $\beta_2$-adrenergic receptor ($\beta$2-AR) activate their cognate G protein in the monomeric form [9–12] and that supramolecular organizations of rhodopsin [9], neurotensin 1 receptor [13] and leukotriene $B_4$ receptor ($BLT_2$) [14] reduce G protein coupling, formation of GPCR oligomers in living cells has been widely demonstrated [15–17]. Indeed, it was recently inferred that the $\beta_2$-AR exists in dynamic equilibrium between monomeric and higher-order oligomers, with the average size of the oligomer being a tetramer and with inverse agonists promoting higher order oligomerization

[15]. The occurrence of oligomeric complexes involving GPCRs and intracellular and extracellular proteins would imply that conformational changes occurring in one receptor molecule in response to ligand binding may be transmitted to others within the multimolecular complex. The conformational changes transmitted by direct protein–protein interactions may represent a first level of regulation of a receptor. The biological role(s) of homologous and heterologous receptor aggregation is/are, however, far from being clarified [18–20]. Likewise, knowledge about the most likely architectures of GPCR dimers is still ill-defined. Sequence- and docking-based approaches investigated dimerization in different GPCRs highlighting the involvement of different helices in the inter-monomer interfaces, with emphasis on helix 4 (H4) [21]. System's dependent variety in the dimer architecture emerges also from results of in vitro experiments. In this respect, the highest resolution information available thus far comes from X-ray crystallography and atomic force microscopy (AFM) measurements on rhodopsin, opsin, $\beta_2$-AR and CXCR4 chemokine receptor, as well as from cysteine crosslinking experiments on $D_2$ receptor ($D_2R$), and disulphide trapping experiments on $5HT_{1c}$ receptor [22–29]. With regard to rhodopsin, the geometrical constraints from AFM measurements led to the proposal of a semi-empirical model of a higher order rhodopsin structure [22]. According to this model, two monomers of rhodopsin interact with each other through the second extracellular loops (EL2), the second cytoplasmic loops (IL2), and H4 and H5 of both monomers. However, rhodopsin crystals obtained under different experimental conditions showed alternative dimeric architectures characterized by H1–H1 or H8–H8 contacts all compatible with the AFM images [23]. A similar architecture was also found for the opsin apoprotein [28]. With respect to the $\beta_2$-AR, crystal packing in the presence of cholesterol shows a significant involvement of the hydrophobic molecule in the inter-monomer interface [24]. In this framework, protein–protein contacts are minimal and include a pair of salt bridges between $K60^{(1.59)}$ (the first number in parenthesis refers to the helix and the following indicate the position of the helical residue relative to the most highly conserved residue within that helix, here denoted as 50, according to the nomenclature proposed by Ballesteros and Weinstein [30]) and E338 from H8 [24]. The crystal structure of CXCR4 in complex with either a small molecule or the CVX15 cyclic peptide antagonist shows a dimer interface essentially contributed by amino acids from the extracellular halves of H5 and H6, with emphasis on the former [29]. Additional contacts involving the cytosolic ends of H3, H4 and IL2 are shown by the CXCR4 complex with the cyclic peptide [29]. For the $D_2R$, cysteine crosslinking experiments interpreted in the context of the structural models highlighted the potential rearrangements of the dimer architecture depending on the receptor functional state, the H4–H5 and H4–H4 contact dimers being, respectively, associated with inactive and active states [25, 26]. In a more recent study, the same authors provided evidence that $D_2R$ forms higher-order oligomers in living cells and that H1 and H8 form a second symmetric interface in addition to the previously identified H4 interface [16]. The involvement of H1/H8 GPCR oligomerization has been recently proposed for the $\beta_2$-AR as well [15]. Finally, recent in vitro disulphide-trapping experiments on the $5HT_{2c}$ receptor suggest the existence of dimer architectures insensitive and sensitive to the functional states of the receptor [27]. In this respect, state-insensitive architectures would involve H1–H1 contacts, whereas state-sensitive architectures would be characterized by H4–H5 contacts [27]. Collectively, consensus emerges on H1, H4 and H5 being involved in GPCR dimerization/oligomerization.

In this study, we predicted the presumable contacts in TP dimers by means of an approach based on docking simulations [31]. Quaternary structure predictions were challenged by in vitro site-directed mutagenesis, immunofluorescence, fluorescence resonance energy transfer (FRET), ligand binding and signaling experiments. In vitro experiments validated the predictions of computational experiments indicating that TP$\alpha$–TP$\beta$ heterodimers are mediated by H1–H1 contacts.

## Experimental procedures

### Materials and methods

Cell-culture media, supplements and sera, and molecular biological reagents, including high fidelity Taq and PCR reagents, were purchased from Invitrogen (San Giuliano Milanese, Italy). Epicurian Coli DH5$\alpha$ competent cells were from Stratagene (La Jolla, CA, USA). Restriction and modification enzymes were purchased from Fermentas/M-Medical (Milan, Italy). Oligonucleotides were synthesized by PRIMM (Milan, Italy) and DNA sequencing was performed by Consorzio di Genetica Molecolare (Monza, Italy). Plasmid DNAs were purified with the QIAprep Spin Miniprep and QIAfilter Plasmid Midi kits (Qiagen, Milan, Italy).

Inositol-free DMEM was from ICN Pharmaceuticals Inc. (Costa Mesa, CA, USA). Ultima Gold was from Packard Instruments (Meriden, CT). [5,6-$^3$H]SQ29,548 and myo-[2-$^3$H]inositol were purchased from Perkin-Elmer (Boston, MA, USA). [1S-[1$\alpha$,2$\alpha$(Z),3$\alpha$,4$\alpha$]]-7-[3-[[2-[(phenylamino) carbonyl]hydrazino]methyl]-7-oxabicyclo[2.2.1]hept-2-yl]-5-heptenoic acid (SQ29,548) and 9,11-dideoxy-9$\alpha$, 11$\alpha$-methanoepoxy-prosta-5Z,13E-dien-1-oic acid (U46619) were from Cayman Chemical (Ann Arbor, MI, USA), and

stored as stock solutions at −20°C. Anion exchange resin AG 1X-8 (formate form, 200–400 mesh), Poly-Prep columns, and Lowry dye-binding protein reagents were from Bio-Rad Laboratories (Hercules, CA, USA). Mouse monoclonal antibody against c-Myc (clone 9E10) and affinity-purified polyclonal antibody anti-human influenza hemagglutinin (HA; Y-11) were form Santa Cruz Biotechnology Inc. (Santa Cruz, CA, USA). All other reagents of the highest purity were from Sigma–Aldrich (St. Louis, MO, USA).

## Computational experiments

Computational experiments consisted in rigid body docking simulations of TPα receptor homodimerization, following a recently reported computational protocol [31–33]. The computational modeling of the TPα receptor is described in detail in a recent publication [34] and consists of comparative modeling followed by ns molecular dynamics (MD) simulations in implicit membrane [34].

In this study, the following structural models of the empty form of the wild-type TP were considered for docking simulations: the selected input structure [($WT_{Inp}$, Table 1), i.e., prior to energy minimization and MD simulation], the energy minimized structure (i.e., prior to MD simulations, $WT_{Min}$, Table 1), the minimized structures averaged over the first, central and last 2 ns (i.e., $WT_{AVGf2ns}$, $WT_{AVGc2ns}$ and $WT_{AVGl2ns}$, respectively, Table 1) as well as the minimized structure averaged over the whole 4-ns trajectory (i.e., $WT_{AVG4ns}$, Table 1).

**Table 1** Results of docking simulations on TP dimerization

| Model[a] | Filtered1[b] | Filtered2[c] | H1–H1 Sol.[d] | Best Sol[e] | $ZD^{f}_{best.}$ |
|---|---|---|---|---|---|
| $WT_{Input}$ | 125 | 44 | 10 | 52 | 19.62 |
| $WT_{Min}$ | 130 | 55 | 7 | 74 | 17.56 |
| $WT_{AVGF2ns}$ | 59 | 13 | 13 | 154 | 16.01 |
| $WT_{AVGC2ns}$ | 92 | 22 | 18 | 99 | 16.62 |
| $WT_{AVGL2ns}$ | 75 | 10 | 8 | 32 | 17.10 |
| $WT_{AVG4ns}$ | 88 | 22 | 15 | 30 | 17.72 |

[a] Structural models of TPα $WT_{Inp}$ and $WT_{Min}$ are, respectively, the input and minimized structures prior to MD simulations; $WT_{AVGf2ns}$, $WT_{AVGc2ns}$ and $WT_{AVGl2ns}$ are, respectively, the minimized structures averaged over the first, central and last 2 ns; $WT_{AVG4ns}$ is the minimized structure averaged over the whole 4-ns trajectory

[b] Number of filtered solutions according to the tilt angle and *z*-offset cutoffs

[c] Final filtered solutions following cluster analysis and visual inspection of the cluster centers

[d] Number of solutions holding H1–H1 contacts

[e] Rank order of the best solution, which is always characterized by H1–H1 contacts

[f] *ZD*-score of the best solution

Rigid-body docking simulations were carried out by means of the ZDOCK 2.1 software [35], following the same protocol detailed in a methodological article [31] In this respect, two identical copies of each structural model were docked together, i.e., one monomer was used as a fixed protein (target) and the other as a mobile protein (probe). A rotational sampling interval of 6° was employed, i.e., dense sampling, and the best 4,000 solutions were retained and ranked according to the ZDOCK score (ZD-score). These solutions were subjected to a filter, the "membrane topology" filter, which discards all the solutions that violate the membrane topology of the protein. For the membrane topology filter to work properly, the two docked structural models must have the appropriate orientation with respect to the putative membrane. This is due to the fact that ZDOCK expresses its docking solutions in terms of a *x*, *y*, *z*-translation and a $R_zR_xR_z$-rotation of the probe. If both target and probe are properly oriented in a membrane parallel to the *XY* plane, the translation along the *z*-axis can be considered as an offset out of the membrane and the $R_x$ component of the rotation as a deviation from the original orientation in the membrane. Indeed the filter discards all the solutions characterized by a deviation angle from the original *z*-axis, i.e., tilt angle, and a displacement of the geometrical center along the *z*-axis, i.e., *z*-offset, above defined threshold values. For the tilt angle and the *z*-offset, thresholds of 0.6 radians and 6.0 Å were, respectively, employed. The filtered solutions from each run were merged with the target protein, leading to an equivalent number of dimers that were subjected to cluster analysis. The Cα-root mean square deviation (Cα-RMSD) threshold for each pair of superimposed dimers was set equal to 3.0 Å. All the amino acid residues in the dimer were included in Cα-RMSD calculations. Since the filter cutoffs were intentionally quite permissive to avoid removal of reliable solutions, due to possible small deviations of the initial orientation from the proper membrane topology, inspection of the cluster centers served to finally discard the remaining unreliable solutions. The predicted dimers were energy refined, following the same energy minimization setup as the one employed for the receptor monomer. The same docking protocol was also applied to a mutated form of $WT_{AVG4ns}$ carrying alanine substitutions for $I25^{(1.33)}$, $W29^{(1.37)}$, $C35^{(1.43)}$, $V36^{(1.44)}$, $L39^{(1.47)}$, $L43^{(1.51)}$, $L44^{(1.52)}$ and $S47^{(1.55)}$. In this respect, two docking simulations were carried out, one using mutated TP as a target and wild-type TP as a probe, and the other using mutant TP both as a target and as a probe.

## Introduction of N-terminal epitope tags

The cDNAs of TPs were subcloned from the original pcDNA3 expression vectors into the pGW1 vector (kindly

provided by Dr. Bice Chini, University of Milan, Italy) containing the HA epitope (YPYDVPDYA), or the c-Myc epitope (DLDYDSVQPY, corresponding to amino acids 12–22 of human c-myc) for recognition with anti-tag specific antibodies. Briefly, the TP cDNAs were amplified by PCR introducing *Asc*I and *Eco*RI recognition sites before and after the open reading frame of TP. The specific primers ensuring the maintenance of the transcription sequence were designed as follows:

- forward primer (suitable for both TPα and TP$\beta$): 5′-GTTGGCGCGCCATGTGGCCCAACG-3′;
- reverse primer for TPα: 5′-CCCGAATTCCTACTGA GCCCGGAGC-3′;
- reverse primer for TP$\beta$: 5′-CGCCGAATTCTCAATC CTTTCTGGACA-3′.

PCR products were digested using *Asc*I and *Eco*RI restriction enzymes and inserted into the purified expression vector of interest that had been opened between the *Asc*I/*Eco*RI polylinker sites using the respective enzymes. The resulting constructs were verified by sequencing.

### Site-directed mutagenesis

Specific base substitutions were introduced into the cDNAs of TPs using a cDNA specifically synthesized by Geneart (Regensburg, Germany) to generate the corresponding TPα and TP$\beta$ TM1 mutant isoforms, each carrying the amino acids I25$^{(1.33)}$, W29$^{(1.37)}$, C35$^{(1.43)}$, V36$^{(1.44)}$, L39$^{(1.47)}$, L43$^{(1.51)}$, L44$^{(1.52)}$ and S47$^{(1.55)}$ in H1 replaced by alanines. The resulting constructs were verified by sequencing.

### Culture and transfection of HEK293T cells

HEK293T cells were cultured in Dulbecco's modified Eagle's medium (DMEM) supplemented with 10% (v/v) fetal bovine serum (FBS), 2 mM glutamine, 50 units/ml penicillin, 100 µg/ml streptomycin at 37°C in a humidified atmosphere of 95% air and 5% $CO_2$. Transfections were performed using the FuGENE6 reagent (Roche Diagnostics, Milan, Italy) following manufacturer's instructions. Briefly, cells were seeded onto tissue culture dishes previously coated with 10 µg/ml poly-D-lysine, and transfected at 50–60% confluency with an optimized 3:1 FuGENE 6/DNA ratio. All analyses were performed 48 h after transfection.

### Immunofluorescence microscopy

Transfected cells on coverslips were incubated for 1 h with anti-Myc or anti-HA antibodies under non-permeabilizing conditions in the absence or presence of U46619 agonist ($10^{-6}$ M) in DMEM plus 10% FBS at 37°C. After treatment, cells were washed twice with PBS/$Ca^{2+}$/$Mg^{2+}$ and fixed for 10 min at 25°C with 4% (w/v) p-formaldehyde in 0.12 M sodium phosphate buffer, pH 7.4. Fixed cells were rinsed with PBS/$Ca^{2+}$/$Mg^{2+}$, incubated for 1 h with Alexa Fluor 488- or 568-conjugated secondary anti-mouse or anti-rabbit IgG antibodies in GDB buffer [0.02 M sodium phosphate buffer, pH 7.4, containing 0.45 M NaCl, 0.2% (w/v) bovine gelatine], washed with PBS/$Ca^{2+}$/$Mg^{2+}$, and mounted on glass slides with a 90% (v/v) glycerol/PBS solution. Samples were analyzed using Zeiss LSM 710 confocal laser-scanning microscope (Jena, Germany). Receptor co-internalization was calculated as the ratios between the average intensities of cytoplasmatic total fluorescence in each cell. Statistical analysis was performed on 30 cells for each experimental condition from three independent transfections.

### Acceptor photobleaching FRET

The FRET measurements were performed with the laser-induced acceptor bleaching method previously reported [36]. Briefly, cells co-transfected with wild-type or mutant HA- and Myc-tagged TP pairs were incubated for 1 h with the anti-tag antibodies, fixed and exposed to fluorochrome-conjugated secondary antibodies. All images were acquired with the laser scanning confocal microscope using a 63× oil-immersion objective applying an additional 1.5–2× zoom. Before bleaching, three images were captured in the 488-nm (donor fluorochrome wavelength) and the 561-nm (acceptor fluorochrome wavelength) channels using the line-by-line sequential mode without any averaging steps to reduce basal bleaching. Then, the defined plasmalemmal region of interest (ROI) was bleached by 20 pulses of full power 561-nm laser line (each pulse 1.28 µs/pixel). After bleaching seven images were acquired to obtain a full curve for analysis. The number of bleaching steps was held constant throughout each experiment. FRET was quantified by measuring the average intensities of ROIs in the donor and acceptor fluorochrome channels before and after bleaching using the NIH ImageJ software (http://rsbweb.nih.gov/ij/). To determine any change of fluorescence intensities not due to FRET occurring during the measurements, a distinct membrane 'sentinel' ROI of approximately the same size of the bleached ROI was measured in parallel, and all the results were normalized according to the background bleaching recorded in the sentinel ROI. Proper controls were performed to verify that no artifacts were generated in the emission spectra throughout the experimental setup due to sample overheating. Twenty measurements from two different transfections were performed for each experimental condition.

### Radioreceptor binding

Receptor expression was monitored by equilibrium mixed type binding curves of [$^3$H]SQ 29,548 (48 Ci/mmol) performed as previously described [37, 38]. Briefly, confluent adherent cells in 250 µl of serum-free DMEM, containing 0.2% (w/v) BSA were assayed in the presence of 0.1–1 nM serial dilutions of [$^3$H]SQ 29,548 and 3 nM–10 µM of the homologous cold ligand. After 30 min incubation at 25°C, cells were lysed in 0.5 N NaOH. Bound ligand was separated by rapid vacuum filtration through a Brandel Cell Harvester (Gaithersburg, MD, USA) onto glass-fiber GF/C filters. Radioactivity was measured by liquid scintillation counting.

### Total inositol phosphate production

Signaling of TPs was assessed by measuring the accumulation of total IPs as previously described [37, 38]. Briefly, cells labeled overnight with 0.5 µCi of *myo*-[2-$^3$H]inositol (18 Ci/mmol) were pre-incubated with 25 mM LiCl for 10 min followed by incubation with increasing concentrations of the TP selective U46619 agonist for 30 min at 37°C. The reaction was terminated by removal of the medium. Total IPs were extracted with 10 mM formic acid for 30 min, neutralized with 5 mM $NH_4OH$, pH 8–9, and purified by anion exchange chromatography through AG 1X-8 resin, formate form, 200–400 mesh.

### Statistical analysis

Analysis of ligand binding data was performed by implementing in Prism 4 (GraphPad Software Inc., San Diego, CA, USA) the model described in the LIGAND software [39]. Statistical analysis of the concentration–response curves was performed with Prism 4 using the four-parameter logistic model, as described in the ALLFIT program [40]. Errors are expressed as percent coefficient of variation (%CV) and calculated by simultaneous analysis of at least two independent experiments performed with duplicate determinations. All curves were fitted by computer.

Statistical analysis of immunofluorescence data was performed using Student *t* test or one-way ANOVA repeated measurements with one grouping factor.

Data are expressed as means ± SD. A level of statistical significance of $p < 0.05$ was accepted.

## Results

### Predictions of likely interfaces in TP dimers

Computational experiments were carried out on structural models of TPα. This isoform (343 residues) shares the first 328 amino acids with TP$\beta$ (407 residues). The exclusion of TP$\beta$ from computational experiments was dictated by difficulties in modeling the 344–407 C-terminal portion that lacks homology with the rhodopsin template. Our choice to focus on TPα is also justified by the founded expectation that quaternary structure predictions on TPα are also valid for TP$\beta$ since the structural differences between the two isoforms are limited to the last 15 amino acids of TP$\beta$ that unlikely participate in inter-monomer contacts. Predictions were carried out by a computational approach based upon rigid-body docking, ad hoc filtering, automatic cluster analysis and visual inspection of the cluster centers (i.e., the structure with the highest number of neighbors in a cluster) (see Materials and methods [31]). In order to corroborate predictions, docking simulations were carried out on six different structural models of the empty wild-type receptor (Table 1, see also Methods).

Collectively, the docking solutions that passed the membrane topology-based filter (i.e., the realistic solutions) range from a minimum of 65 to a maximum of 125 out of the 4,000 collected from each run (Table 1), thus representing on average about 2% of the total output solutions (i.e., the best solutions according to the docking score (*ZD*-score). Since the filtering conditions were intentionally quite permissive (see Materials and methods), inspection of the cluster centers finally served to discard the remaining low reliable solutions. Following this final filtering the percentage of reliable solutions decreased on average to 0.7%. For all the docking simulations on the different average minimized structures, more than 60% of such reliable solutions are characterized by H1-H1 contacts. Among them, the best solutions (i.e., according to the docking score) fall among the first 100 out of 4,000, and share a common architecture of the inter-monomer interface, characterized by H1–H1 and, to a lower extent, by H1–H2,EL1 and H8–H8 contacts (Table 1, Supplementary Figure 1 (Figure S1)). This is true for all the forms except $WT_{AVGF2ns}$ for which the best solution has a rank number 154 and is characterized by lack of H8–H8 contacts (Figure S1C). The predicted interface involves also contacts between a limited number of amino acids from the N-terminus (Fig. 1). Most of the inter-monomer contacts involve hydrophobic amino acids on transmembrane H1 (TM1) from both dimers. Monomers A and B in the predicted dimer (i.e., docking solution N. 30, Table 1; Figs. 1, S1F) bury 1,412 and 1,418 Å$^2$ of surface, respectively. The contribution of N-ter, H1, H2, E1, and H8 to the total buried surface area in the predicted monomer is 11.62, 33.07, 18.20, 15.41, and 21.70%, respectively.

Alanine replacements of the H1 amino acids participating in inter-monomer interface in the predicted dimer, i.e., $I25^{(1.33)}$, $W29^{(1.37)}$, $C35^{(1.43)}$, $V36^{(1.44)}$, $L39^{(1.47)}$, $L43^{(1.51)}$, $L44^{(1.52)}$ and $S47^{(1.55)}$, resulted in changes in

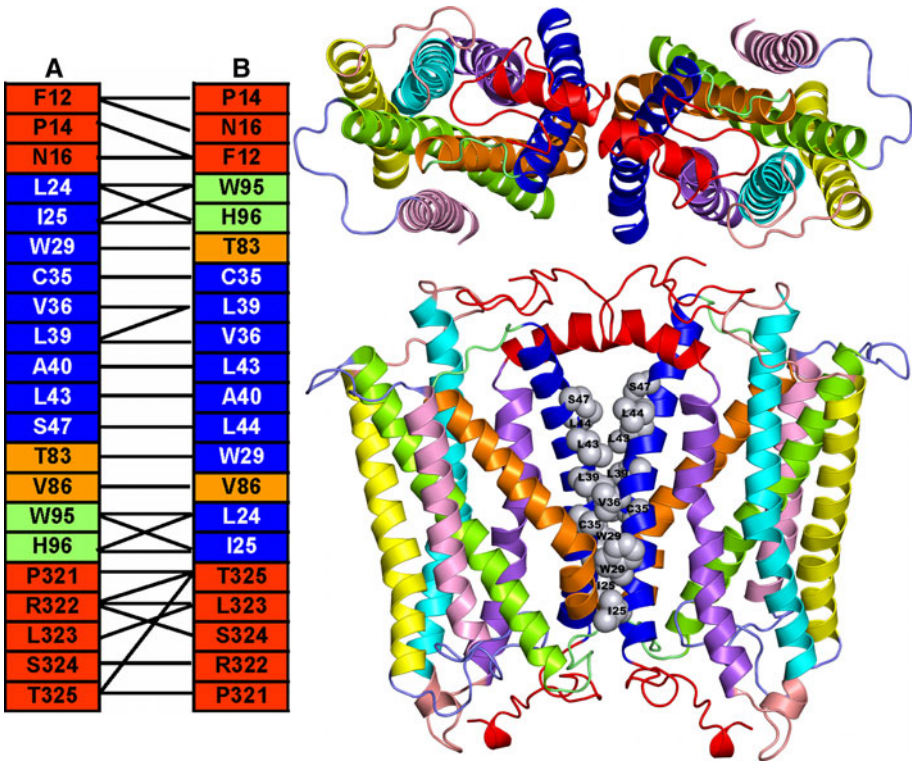


**Fig. 1** Predicted dimeric model of TPα. The predicted dimer is the solution N. 30 derived from docking simulations on the minimized structure averaged over the whole 4-ns trajectory. *Left* amino acids that contribute to the inter-monomer interface are shown. **a** −0.5 kcal $mol^{-1}$ interaction energy cutoff was chosen to connect amino acids. *Squares* are colored according to the amino acid location (see above in the legend). Squares corresponding to N-ter and EL1, receptor portions not shown in the *top panel*, are *red* and *lime*, respectively. *Drawings* were done by means of the software PYMOL 0.97 (http://pymol.sourceforge.net/). *Right cartoon* representation of the predicted dimeric model of TPα, seen from the intracellular side in a direction perpendicular to the membrane surface (*top*) as well as in a direction parallel to the membrane surface (*bottom*) are shown. The extracellular loops are not shown in the *top image*. H1, H2, H3, H4, H5, H6, H7 and H8 are, respectively, *blue*, *orange*, *green*, *pink*, *yellow*, *cyan*, *violet* and *red*. IL1 and EL1 are *lime*, IL2 and EL2 are *slate*, IL3 and EL3 are *salmon* and the N- and C-terms are *red*. In the *bottom image*, the side chains of the interface amino acids subjected to alanine substitutions are shown in *gray*

number and docking scores of the reliable solutions. In particular, docking simulations using mutant TP as a target and WT TP as a probe, found the same docking solution as simulations on the corresponding wild-type form but with a decreased docking score (i.e., solution N. 195 was the best one). On the other hand, docking simulations using mutant TP both as a target and as a probe resulted in a significant reduction in number and docking score of the reliable solutions. Indeed, only three reliable solutions over 4,000 could be found, characterized by the same architecture of the predicted dimer of wild-type TP but with significantly higher rank numbers, i.e., 543, 2,388, and 3,324. Collectively, these data suggest that the integrity of H1 is required for the achievement of reliable dimeric architectures.

## Cell expression of wild-type and TM1 mutant TPα and TPβ

To challenge the predictions of computational modeling on the contact interfaces in TPα and/or TPβ homodimers and heterodimers we replaced $I25^{(1.33)}$, $W29^{(1.37)}$, $C35^{(1.43)}$, $V36^{(1.44)}$, $L39^{(1.47)}$, $L43^{(1.51)}$, $L44^{(1.52)}$ and $S47^{(1.55)}$ with alanines and generated the corresponding N-terminal Myc- and HA-epitope tagged versions of TM1 mutant TPα and TPβ, respectively.

We then analyzed the levels of the TM1 mutants individually expressed in transiently transfected HEK293T cells. The binding of the selective TP antagonist [$^3$H]-SQ29,548 to intact cells expressing the TM1 mutant TPα or TPβ was found to be severely reduced compared to the corresponding wild-type receptors (about 60 and 80%, respectively; data not shown). Thus, in all subsequent experiments, transfection conditions were adjusted to ensure comparable levels of expression of wild-type and mutant receptors in a range between 1–3 and 0.2–0.8 pmol/mg protein for TPα and TPβ, respectively. Mock transfected cells showed no detectable binding of [$^3$H]-SQ29,548 in mixed type curves (data not shown), whereas cells transfected with wild-type TPα displayed a monophasic binding curve fitting to a single site model by

computer analysis, with binding parameters as previously reported [37, 41]. TM1 mutant TPα and TPβ displayed binding affinities not statistically different from the corresponding wild-type receptors. In fact, the [$^3$H]-SQ29,548 dissociation constants ($K_d$) of wild-type and TM1 mutant TPα are, respectively, 37.73 ± 13.46 and 17.44 ± 15.97 nM ± %CV, and those for wild-type and TM1 mutant TPβ are 13.30 ± 13.27 and 5.53 ± 16.92 nM ± %CV, respectively.

## Validation of in silico predictions: effect of TM1 mutations on hetero-dimerization of TPα and TPβ

It has been previously reported that TPβ undergoes agonist-induced endocytosis with a kinetics similar to many GPCRs, whereas TPα does so only after prolonged (2–4 h) agonist stimulation, or when co-expressed in the same cells with TPβ [4], or prostacyclin receptor (IP) [7]. These observations suggested that TPα associates with TPβ or IP, thus forming hetero-dimeric receptor complexes that undergo agonist-promoted intracellular trafficking. TM1 mutations did not alter the trafficking of individually expressed TPα and TPβ in response to agonist stimulation. The addition of $10^{-6}$ M U46619 agonist to HEK293T cells for 60 min caused the internalization of both wild-type and TM1 mutant TPβ, whereas both wild-type and TM1 mutant TPα retained their plasma membrane localization (Fig. 2). When wild-type HA-tagged TPα and Myc-tagged TPβ were co-expressed in HEK293T cells, they both localized at the cell surface at steady state, and in intracellular puncta following exposure to $10^{-6}$ M U46619 agonist for 15–60 min (Fig. 3), thus confirming the co-internalization of TP heterodimers previously reported [4]. Remarkably, after performing the same experiment with the corresponding TM1 mutants, some co-localization of TPα and TPβ could be still detected at the membrane of unstimulated cells, but intracellular puncta were uniquely labeled by TPβ fluorescence following stimulation with agonist (Fig. 3). Likewise, the agonist-induced internalization of TM1 TPα did not occur when co-expressed with wild-type TPβ, and wild-type TPα failed to internalize when co-expressed with TM1 TPβ. These results suggest that independently from which TP member of the co-transfected pair contains the TM1 mutations the TPβ–TPα association is impaired and, consequently, also the co-internalization of TPα with TPβ.

To obtain direct evidence that TM1 mutations impair TPα–TPβ dimerization we performed the FRET analysis by using the laser-induced acceptor bleaching method reported by König et al. [36]. This type of analysis is based on the fact that when energy transfer occurs, the fluorescence emission by the donor fluorochrome is quenched because of the direct transfer of excitation energy to the acceptor

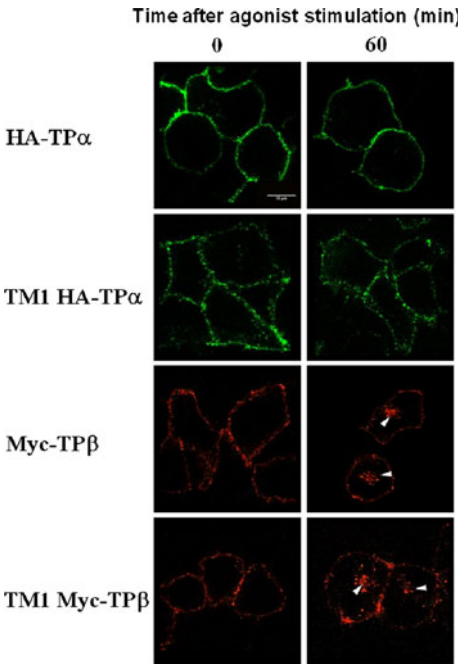


**Fig. 2** Cellular localization of recombinant wild-type and TM1 mutant TPα and TPβ following cell exposure to agonist. HEK293T cells transiently transfected 48 h before with either wild-type or TM1 mutant HA-tagged TPα or Myc-tagged TPβ were exposed to $10^{-6}$ M U46619 agonist for 60 min. After fixation with 4% *p*-formaldehyde indirect immunofluorescence was performed with anti-tag antibodies and results visualized using laser scanning confocal microscopy. Clearly, wild-type and TM1 mutant TPβ undergo agonist-induced internalization upon agonist exposure (*arrowheads* pointing to intracellular puncta) whereas wild-type and TM1 mutant TPα maintain their localization at the plasma membrane. *Scale bar* 15 μm. Results are representative of ten fields analyzed for each of three independent experiments

fluorochrome. If the acceptor fluorochrome is fully bleached by laser, FRET is blunted and the donor signal is de-quenched, thus resulting in an enhanced fluorescence emission by donor fluorochrome. Thus, HEK293T cells on coverslips were co-transfected with different combinations of wild-type or TM1 mutant HA-TPα and Myc-TPβ pairs. Two days after transfection the cells were incubated with anti-epitope antibodies then fixed and exposed to secondary antibodies conjugated to donor and acceptor fluorochromes. Cell samples, imaged under confocal microscope, were subjected to laser-induced bleaching of acceptor fluorescence in defined plasma membrane ROIs. Before and after bleaching donor and acceptor fluorescences were recorded over time. Figure 4 shows that an increase of fluorescence signal emitted by the donor fluorochrome resulting from de-quenching (i.e., FRET signal) was only evident in cells co-expressing the wild-type TPα–TPβ pair whereas no increase occurred in cells expressing either the TM1 mutant pair, or one wild-type TP and one TM1 TP. These results suggest that TM1 mutation in either TPα or TPβ, is sufficient to undermine hetero-dimerization of the two isoforms.

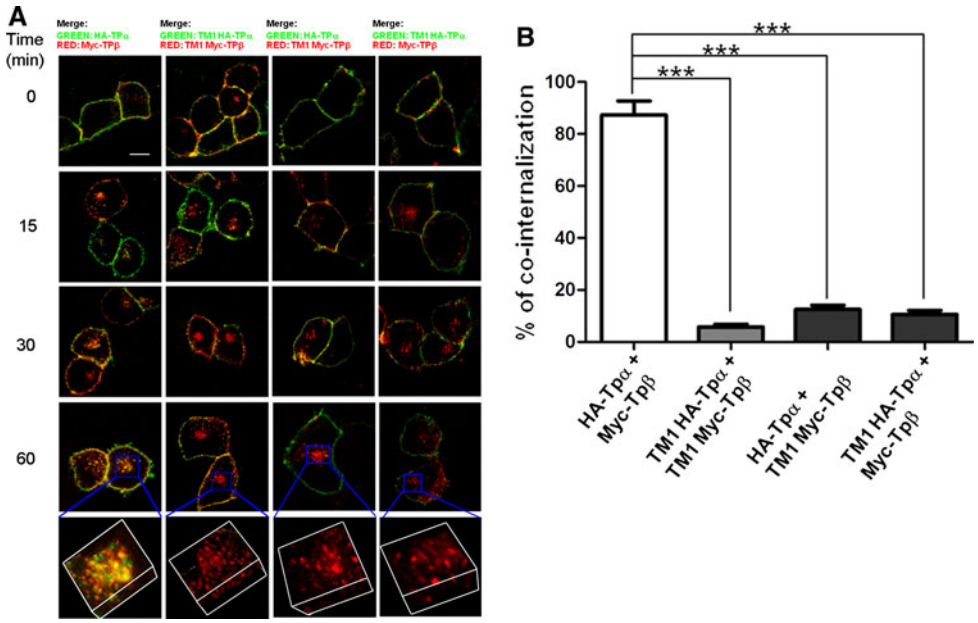


**Fig. 3** Time-course of the effect of agonist exposure on the subcellular localization of co-expressed TPα and TP$\beta$ pairs in transfected HEK293T cells. HEK293T cells were transiently co-transfected with different combinations of wild-type or TM1 mutant HA-tagged TPα and Myc-tagged TP$\beta$ pairs. **a** Upon cell exposure to $10^{-6}$ M U46619 agonist for different times (15–60 min), wild-type HA-TPα co-internalized with wild-type Myc-TP. In contrast, agonist-dependent stimulation of cells co-expressing TM1 TPα together with TM1 or wild-type TP$\beta$ caused the internalization of only the TP$\beta$ while leaving unaffected the plasma membrane localization of TM1 TPα (*green surface*). Also wild-type TPα failed to undergo agonist-induced internalization when co-transfected with TM1 TP$\beta$. Images are representative of four independent experiments, ten microscope fields for each experiment. *Scale bar* 15 μm. *Lowest panels* show the 3D reconstructions of 23 optical slices (5 μm total thickness) of internalization vesicles after 60 min agonist stimulation of HEK293T cells transiently co-transfected with corresponding TPα and TP$\beta$ pairs. The reconstructions clearly show that wild-type TPα was co-localized in intracellular vesicles (yellow puncta) only when co-expressed with wild-type TP$\beta$. The absence of yellow vesicles in cells co-expressing TM1 TPα together with TM1 or wild-type TP$\beta$, or in cells co-expressing wild-type TPα and TM1 TP$\beta$ does not depend on the selected focal plane. **b** The histogram shows the average fluorescence intensities of wild-type and TM1 mutant TPα co-internalized with corresponding TP$\beta$ following 60 min agonist exposure. Results are expressed as mean values ± SD. Statistical analysis was performed using the one-way ANOVA test. $^{**}p < 0.01$

### Signaling of TPα and TP$\beta$ wild-type and TM1 mutants

We compared the functional activities of wild-type and TM1 mutant receptors by measuring the U46619 agonist-induced accumulation of IPs in HEK293T cells transiently expressing comparable levels of TP isoforms. Basal IP levels were not significantly different in cells expressing wild-type or TM1 mutant receptors (Table 2). Also the efficacy of $10^{-6}$ M U46619 to elicit an increased IP accumulation (>10-fold increase over basal) was similar for cells expressing the wild-type or the TM1 mutant receptors. In contrast, computer-assisted analysis of concentration–response curves evidenced a 20-fold difference between the $EC_{50}$ values of agonist stimulation of wild-type and TM1 mutant TPα ($EC_{50}$ wild-type = 12.9 nM ± 20.7%CV; $EC_{50}$ TM1 = 210 nM ± 15.7%CV; $p < 0.01$) (Fig. 5). Likewise, U46619 stimulated TM1-TP$\beta$ at approximately tenfold less potency than wild-type TP$\beta$ ($EC_{50}$ wild-type = 26.5 nM ± 25.7%CV; $EC_{50}$ TM1 = 228 ± 12.6) (Fig. 5).

## Discussion

A growing number of in vitro evidence supports the hypothesis that many GPCRs assemble in homo- or hetero-dimeric/oligomeric complexes [3]. The functional role of such supra-molecular complexes is still unclear and may vary depending on the GPCR type [18, 20]. In particular, for TP, the formation of TPα–TP$\beta$ and TPα–IP heterodimers in constitutive human systems seems to greatly influence their pharmacological profiles [4–6], whereas no data are yet available on the functional significance of TP homodimerization. On the same line, the molecular architecture of either homodimers or heterodimers of TP is still obscure.

In this study, we have employed an integrated approach of in silico and in vitro experiments to infer high-resolution information on TP homodimers and heterodimers, whose existence had been previously reported [4]. In this respect, in vitro experiments were employed to validate a clear inference from computational experiments. The latter

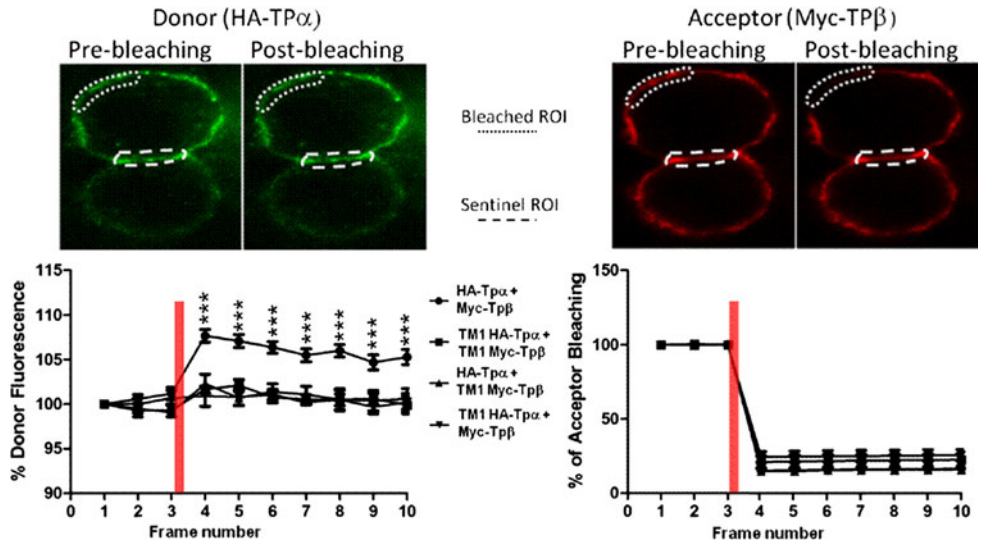


**Fig. 4** Acceptor photobleaching FRET analysis of HEK293T cells transiently expressing wild-type or TM1 mutant TPα and TP$\beta$ pairs. HEK293T cells co-transfected with wild-type or TM1 mutant HA-TPα and Myc-TP$\beta$ pairs were labeled in vivo with the corresponding anti-tag antibodies. After fixation the cells were subjected to indirect immunofluorescence with Alexa Fluor 488- (donor fluorochrome) or 568 (acceptor fluorochrome)-conjugated secondary antibodies and imaged with laser scanning confocal microscopy. *Upper panels* show representative images of fluorescent signals emitted by donor- (HA-TPα; *green*) and acceptor (Myc-TP$\beta$; *red*) fluorochromes in two contiguous HEK293T cells expressing wild-type HA-TPα and Myc-TP$\beta$ pairs before and after laser-induced photobleaching of acceptor fluorescence in a defined plasma membrane region of interest (ROI; *dotted line*). The *lower panels* show the quantification of average percent donor and acceptor fluorescence intensities of wild-type and TM1 mutant HA-TPα and Myc-TP$\beta$, respectively, normalized for unbleached 'sentinel' plasma membrane ROIs (*broken line*). A statistically significant (***$p < 0.001$; $n = 20$) increase of wild-type versus TM1 mutant HA-TPα donor signal is measured for all recorded post-bleaching captured frames. The decrease of wild-type and TM1 Myc-TP$\beta$ acceptor signals are not significantly different. Statistical analysis of immunofluorescence data was performed using one-way ANOVA repeated measurements with one grouping factor. Data are expressed as means ± SD

**Table 2** Basal IP levels of TPα or TP$\beta$ wild-type and TM1 mutants

| Receptor | Basal dpm ± SD |
|---|---|
| TPα | 7,260 ± 330 |
| TM1 TPα | 7,446 ± 229 |
| TP$\beta$ | 6,320 ± 297 |
| TM1 TP$\beta$ | 5,940 ± 178 |

relied on quaternary structure predictions of transmembrane proteins, based upon rigid body docking simulations, membrane topology-based filtering, and cluster analysis [31–33]. Predictions from six independent docking simulations on different structural models of the TPα receptor highlighted the interface essentially characterized by contacts between amino acids distributed along the entire main axis of H1 as the best scored and reliable one (Fig. 1). Due to the common architecture shared by the members of the rhodopsin GPCR family, extensive H1–H1 contacts would imply also contacts between the C-terminal portion of H8, leading to an H1–H1, H8–H8 dimer (Fig. 1). Remarkably, such prediction is expected to apply also to TP$\beta$ homodimers and TPα–TP$\beta$ heterodimers as the two isoforms share the first 328 amino acids that include all the residues in the predicted interface, expected to perform the bulk of the inter-monomer contacts. Since computational experiments predict that H1 drives TP dimer formation, we engineered a TP mutant characterized by alanine replacements of the TM1 amino acids involved in most of the inter-monomer interface. If quaternary structure predictions were correct, we would expect an impairment of dimerization. In vitro experiments probed the effects of TM1 mutation on TPα–TP$\beta$ cross-talk. The first validation in this respect came from the observations that wild-type and TM1 TPα did not undergo endocytosis following agonist stimulation when co-expressed with TM1 TP$\beta$, as well as wild-type TPα failed to internalize when co-expressed with TM1 TP$\beta$ (Fig. 3). The agonist-promoted internalization of wild-type TPα only occurred when co-expressed with wild-type TP$\beta$ (Fig. 3) [4]. The impairment of TPα internalization when itself or the partner TP$\beta$ holds the TM1 mutations could arise either from the inability of the TM1 mutant to form hetero-dimeric complex required for TPα to be co-internalized with TP$\beta$, or from the mutational disruption of the interaction between TP and unknown protein(s) of the endocytic machinery. The fact that TM1 mutant TP$\beta$ still retains its ability to internalize and the direct assessment of hetero-dimerization by acceptor photobleaching FRET analysis (Fig. 4) support the view that indeed TM1 mutations in only one member of the pair is enough to impair the association between TPα and TP$\beta$.

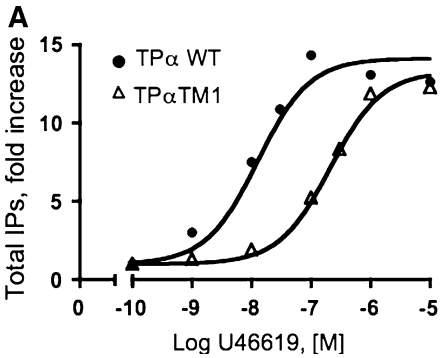


B

| | $EC_{50}$, nM ± %CV | |
|---|---|---|
| | WT | TM1 |
| TPα | 12.9 ± 20.7 | 210** ± 15.7 |
| TPβ | 26.5 ± 25.7 | 228** ± 12.6 |

**Fig. 5** Agonist-induced IP accumulation in HEK29T3 cells transiently expressing the wild-type and mutant TPα and TP$\beta$. **a** Concentration–response curve of U46619 (30 min) in cells expressing wild-type and TM1 mutant TPα. Total IP are expressed as fold increase versus maximal response induced by $10^{-6}$ M U46619 stimulation of wild-type receptor (73,770 dpm ± 1,970 SD, set as 100%). Parameters were obtained by simultaneous computer analysis of three independent experiments, each performed with duplicate determinations. For clarity, only one representative computer-generated curve for each receptor is shown. **b** $EC_{50}$ values of wild-type and TM1 mutant TPα and TP$\beta$. Data are expressed as means ± SD $^{**}p < 0.01$

Preliminary experiments showed reduced membrane expression for both TM1 mutant TPα and TP$\beta$ with respect to their wild-type counterparts (data not shown). A reduced surface expression had been already observed for other TP receptor mutants (Capra et al. [37] and unpublished observations). This can be interpreted as either a reduction in receptor stability, or misfolding, or inability of the mutant receptors to pass the cell quality control, and/or to be efficiently transported to the cell surface [42]. Nonetheless, the mutant TPs that reached the plasma membrane bound the antagonist [$^3$H]-SQ29,548 with normal affinity, and could be activated by the stable $TXA_2$ agonist U46619 as efficiently as the wild-type receptors at equal level of expression. These data are consistent with the observation that monomeric GPCRs are the minimal functional unit in G protein activation and that dimerization/oligomerization is not absolutely required for this process [9–14, 43]. However, the U46619 agonist, stimulated TM1 mutant TPα and TP$\beta$ with a marked reduction in potency, thus suggesting that dimer formation favors a more efficient signaling complex. Since the inter-monomer interface is the same for homodimers and heterodimers, it is expected that there would be no differences in agonist potencies for all dimer types. Indeed, this has already been confirmed by us and others [5].

Hetero-dimerization is thought to regulate TPα function through agonist-induced internalization. In this respect, given that monomers and homodimers are, presumably, in equilibrium at steady state, it is likely that when a TPα monomer makes complexes with a TP$\beta$ or IP protomer there would be a shift in the equilibrium from TPα homodimers to monomers with a consequent overall decrease in agonist potency (Fig. 5), which can be important in cardiovascular homeostasis.

Collectively, the combination of in silico and in vitro experiments indicates that TPα–TP$\beta$ heterodimers are characterized by H1–H1 contacts. This is consistent with emerging evidence from structure determinations, structure predictions and in vitro experiments on homologous GPCRs, suggesting that H1 is likely to be a privileged mediator of dimerization/oligomerization of these membrane proteins [15, 16, 23, 24, 27, 28, 32]. The architecture of the predicted TP dimers is such that it is likely shared by both TPα and TP$\beta$ homodimers as well as TPα–TP$\beta$ heterodimers.

The combined in silico and in vitro approach employed in this study can be adopted to gain structural and functional insights into the dimerization/oligomerization process of all GPCRs for which the structural model of the monomer can be achieved at reasonable atomic resolution.

**Acknowledgments** This work was supported by grants from the Telethon-Italy Grant No. S00068TELU to F.F., the Italian Ministry for University and Research (MiUR-FIRB Grant No. RBIN04CKYN) to M.P., and from European Community Framework Program 6 (No. LSHM-CT-2004-005033) and Fondazione Banca del Monte di Lombardia to G.E.R.

## References

1. Lefkowitz RJ (2000) The superfamily of heptahelical receptors. Nat Cell Biol 2:E133–E136
2. Gurevich VV, Gurevich EV (2008) GPCR monomers and oligomers: it takes all kinds. Trends Neurosci 31:74–81
3. Terrillon S, Bouvier M (2004) Roles of G-protein-coupled receptor dimerization. EMBO Rep. 5:30–34
4. Laroche G, Lepine MC, Theriault C, Giguere P, Giguere V, Gallant MA, de Brum-Fernandes A, Parent JL (2005) Oligomerization of the alpha and beta isoforms of the thromboxane A2 receptor: relevance to receptor signaling and endocytosis. Cell Signal 17:1373–1383
5. Wilson SJ, McGinley K, Huang AJ, Smyth EM (2007) Heterodimerization of the alpha and beta isoforms of the human thromboxane receptor enhances isoprostane signaling. Biochem Biophys Res Commun 352:397–403

6. Wilson SJ, Roche AM, Kostetskaia E, Smyth EM (2004) Dimerization of the human receptors for prostacyclin and thromboxane facilitates thromboxane receptor-mediated cAMP generation. J Biol Chem 279:53036–53047
7. Wilson SJ, Dowling JK, Zhao L, Carnish E, Smyth EM (2007) Regulation of thromboxane receptor trafficking through the prostacyclin receptor in vascular smooth muscle cells: role of receptor heterodimerization. Arterioscler Thromb Vasc Biol 27:290–296
8. Cheng Y, Austin SC, Rocca B, Koller BH, Coffman TM, Grosser T, Lawson JA, FitzGerald GA (2002) Role of prostacyclin in the cardiovascular response to thromboxane A2. Science 296:539–541
9. Bayburt TH, Leitz AJ, Xie G, Oprian DD, Sligar SG (2007) Transducin activation by nanoscale lipid bilayers containing one and two rhodopsins. J Biol Chem 282:14875–14881
10. Ernst OP, Gramse V, Kolbe M, Hofmann KP, Heck M (2007) Monomeric G protein-coupled receptor rhodopsin in solution activates its G protein transducin at the diffusion limit. Proc Natl Acad Sci USA 104:10859–10864
11. Whorton MR, Bokoch MP, Rasmussen SG, Huang B, Zare RN, Kobilka B, Sunahara RK (2007) A monomeric G protein-coupled receptor isolated in a high-density lipoprotein particle efficiently activates its G protein. Proc Natl Acad Sci USA 104:7682–7687
12. Whorton MR, Jastrzebska B, Park PS, Fotiadis D, Engel A, Palczewski K, Sunahara RK (2008) Efficient coupling of transducin to monomeric rhodopsin in a phospholipid bilayer. J Biol Chem 283:4387–4394
13. White JF, Grodnitzky J, Louis JM, Trinh LB, Shiloach J, Gutierrez J, Northup JK, Grisshammer R (2007) Dimerization of the class A G protein-coupled neurotensin receptor NTS1 alters G protein interaction. Proc Natl Acad Sci USA 104:12199–12204
14. Arcemisbehere L, Sen T, Boudier L, Balestre MN, Gaibelet G, Detouillon E, Orcel H, Mendre C, Rahmeh R, Granier S, Vives C, Fieschi F, Damian M, Durroux T, Baneres JL, Mouillac B (2010) Leukotriene BLT2 receptor monomers activate the G(i2) GTP-binding protein more efficiently than dimers. J Biol Chem 285:6337–6347
15. Fung JJ, Deupi X, Pardo L, Yao XJ, Velez-Ruiz GA, Devree BT, Sunahara RK, Kobilka BK (2009) Ligand-regulated oligomerization of beta(2)-adrenoceptors in a model lipid bilayer. EMBO J 28:3315–3328
16. Guo W, Urizar E, Kralikova M, Mobarec JC, Shi L, Filizola M, Javitch JA (2008) Dopamine D2 receptors form higher order oligomers at physiological expression levels. EMBO J 27:2293–2304
17. Milligan G (2006) G-protein-coupled receptor heterodimers: pharmacology, function and relevance to drug discovery. Drug Discov Today 11:541–549
18. Gurevich VV, Gurevich EV (2008) How and why do GPCRs dimerize? Trends Pharmacol Sci 29:234–240
19. Milligan G (2008) A day in the life of a G protein-coupled receptor: the contribution to function of G protein-coupled receptor dimerization. Br J Pharmacol 153(Suppl 1):S216–S229
20. Prinster SC, Hague C, Hall RA (2005) Heterodimerization of g protein-coupled receptors: specificity and functional significance. Pharmacol Rev 57:289–298
21. Simpson LM, Taddese B, Wall ID, Reynolds CA (2010) Bioinformatics and molecular modelling approaches to GPCR oligomerization. Curr Opin Pharmacol 10:30–37
22. Liang Y, Fotiadis D, Filipek S, Saperstein DA, Palczewski K, Engel A (2003) Organization of the G protein-coupled receptors rhodopsin and opsin in native membranes. J Biol Chem 278:21655–21662
23. Lodowski DT, Salom D, Le Trong I, Teller DC, Ballesteros JA, Palczewski K, Stenkamp RE (2007) Crystal packing analysis of Rhodopsin crystals. J Struct Biol 158:455–462
24. Cherezov V, Rosenbaum DM, Hanson MA, Rasmussen SG, Thian FS, Kobilka TS, Choi HJ, Kuhn P, Weis WI, Kobilka BK, Stevens RC (2007) High-resolution crystal structure of an engineered human beta2-adrenergic G protein-coupled receptor. Science 318:1258–1265
25. Guo W, Filizola M, Weinstein H, Javitch JA (2005) Crosstalk in G protein-coupled receptors: changes at the transmembrane homodimer interface determine activation. Proc Natl Acad Sci USA 102:17495–17500
26. Guo W, Shi L, Javitch JA (2003) The fourth transmembrane segment forms the interface of the dopamine D2 receptor homodimer. J Biol Chem 278:4385–4388
27. Mancia F, Assur Z, Herman AG, Siegel R, Hendrickson WA (2008) Ligand sensitivity in dimeric associations of the serotonin 5HT2c receptor. EMBO Rep 9:363–369
28. Park JH, Scheerer P, Hofmann KP, Choe HW, Ernst OP (2008) Crystal structure of the ligand-free G-protein-coupled receptor opsin. Nature 454:183–187
29. Wu B, Chien EY, Mol CD, Fenalti G, Liu W, Katritch V, Abagyan R, Brooun A, Wells P, Bi FC, Hamel DJ, Kuhn P, Handel TM, Cherezov V, Stevens RC (2010) Structures of the CXCR4 Chemokine GPCR with small-molecule and cyclic peptide antagonists. Science
30. Ballesteros JA, Weinstein H (1995) Integrated methods for the construction of three-dimensional models and computational probing of structure-function relations in G protein-coupled receptors. Methods Neurosci 25:366–428
31. Casciari D, Seeber M, Fanelli F (2006) Quaternary structure predictions of transmembrane proteins starting from the monomer: a docking-based approach. BMC Bioinformatics 7:340
32. Casciari D, Dell'Orco D, Fanelli F (2008) Homodimerization of neurotensin 1 receptor involves helices 1, 2, and 4: insights from quaternary structure predictions and dimerization free energy estimations. J Chem Inf Model 48:1669–1678
33. Fanelli F (2007) Dimerization of the lutropin receptor: insights from computational modeling. Mol Cell Endocrinol 260–262: 59–64
34. Raimondi F, Seeber M, De Benedetti PG, Fanelli F (2008) Mechanisms of inter- and intra-molecular communication in GPCRs and G proteins J. Am Chem Soc 130:4310–4325
35. Chen R, Weng Z (2003) A novel shape complementarity scoring function for protein–protein docking. Proteins 51:397–408
36. Konig P, Krasteva G, Tag C, Konig IR, Arens C, Kummer W (2006) FRET-CLSM and double-labeling indirect immunofluorescence to detect close association of proteins in tissue sections. Lab Invest 86:853–864
37. Capra V, Veltri A, Foglia C, Crimaldi L, Habib A, Parenti M, Rovati GE (2004) Mutational analysis of the highly conserved ERY motif of the thromboxane A2 receptor: alternative role in G protein-coupled receptor signaling. Mol Pharmacol 66:880–889
38. Ambrosio M, Fanelli F, Brocchetti S, Raimondi F, Mauri M, Rovati GE, Capra V (2010) Superactive mutants of thromboxane prostanoid receptor: functional and computational analysis of an active form alternative to constitutively active mutants. Cell Mol Life Sci. doi:10.1007/s00018-00010-00368-00019
39. Munson PJ, Rodbard D (1980) Ligand: a versatile computerized approach for characterization of ligand-binding systems. Anal Biochem 107:220–239
40. De Lean A, Munson PJ, Rodbard D (1978) Simultaneous analysis of families of sigmoidal curves: application to bioassay, radioligand assay, and physiological dose-response curves. Am J Physiol 235:E97–E102
41. Habib A, Vezza R, Creminon C, Maclouf J, FitzGerald GA (1997) Rapid, agonist-dependent phosphorylation in vivo of

human thromboxane receptor isoforms. Minimal involvement of protein kinase C. J Biol Chem 272:7191–7200
42. Margeta-Mitrovic M, Jan YN, Jan LY (2000) A trafficking checkpoint controls GABA(B) receptor heterodimerization. Neuron 27:97–106
43. Kuszak AJ, Pitchiaya S, Anand JP, Mosberg HI, Walter NG, Sunahara RK (2009) Purification and functional reconstitution of monomeric mu-opioid receptors: allosteric modulation of agonist binding by Gi2. J Biol Chem 284:26732–26741